Structure of tubular halloysite-(10 Å) and its transition to -(7 Å) by infrared spectroscopy and X-Ray diffraction

Supplemental Information

Eirini Siranidi[1], Stephen Hillier[2,3] and Georgios D. Chryssikos[1,*]

[1]Theoretical and Physical Chemistry Institute, National Hellenic Research Foundation, 48 Vass. Constantinou Ave., Athens, Greece 11635
[2] The James Hutton Institute, Craigiebuckler, Aberdeen, AB15 8QH
[3]Department of Soil and Environment, Swedish University of Agricultural Sciences, P.O. Box 7014, SE-75007 Uppsala, Sweden

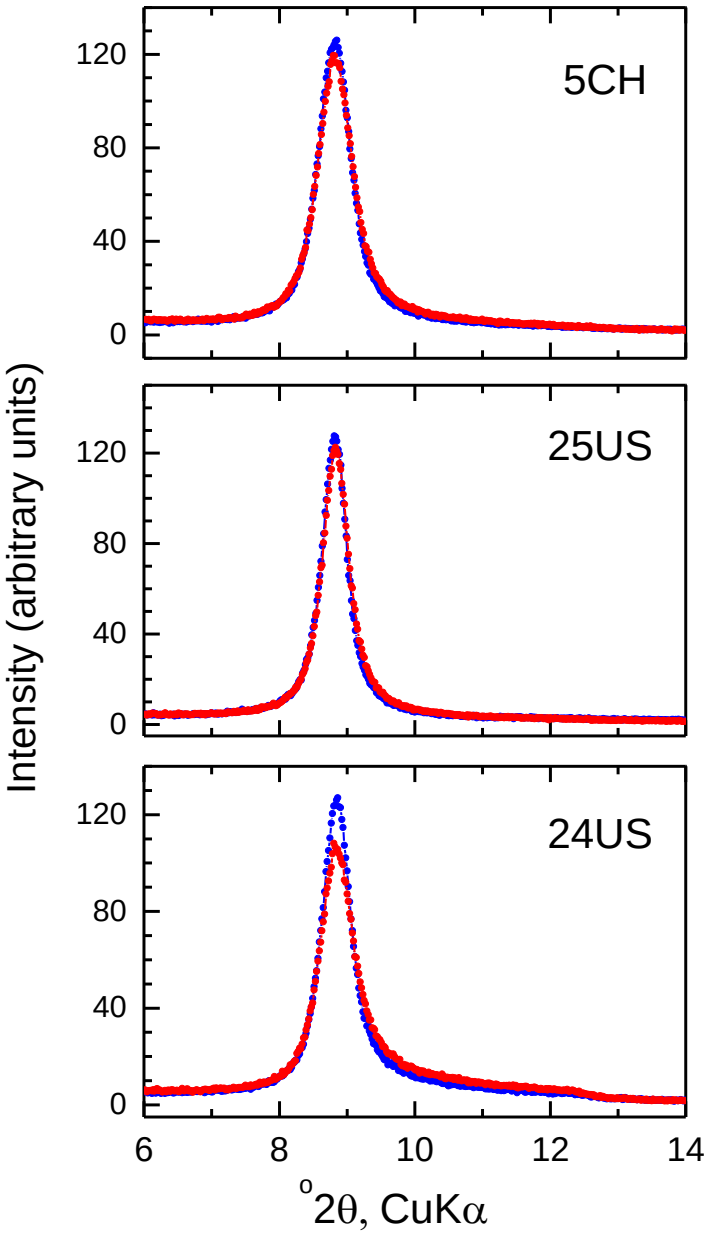

Figure S1. XRD of representative cylindrical (5CH, 25US) and polygonal (24US) halloysite-(10 Å) samples run immediately in the wet/damp state (blue) and following drying at 70 RH% for 3 days at ambient temperature (red).

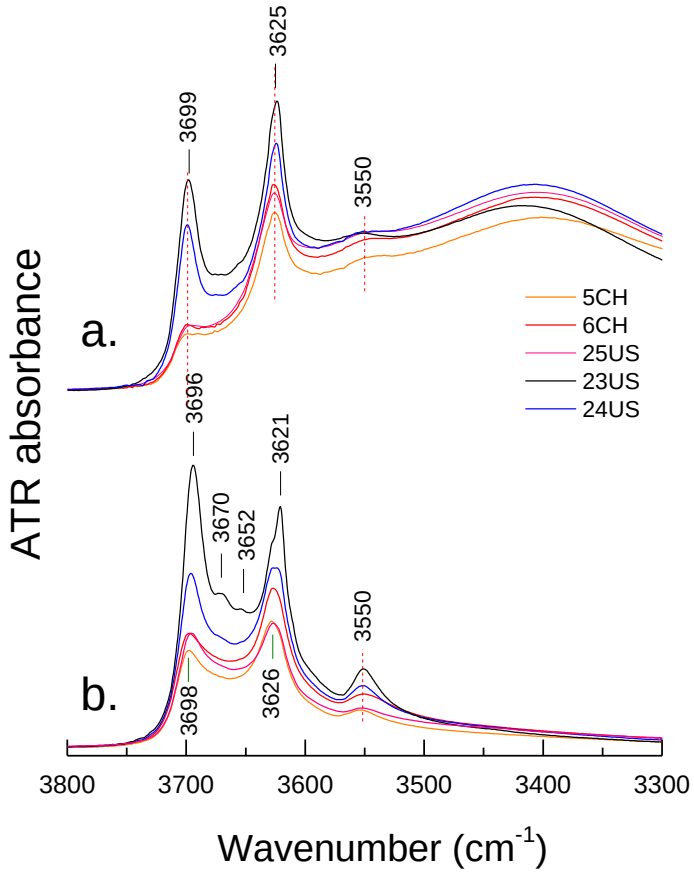

Figure S2. Detail of the ATR spectra of Fig. 3 comparing the five halloysites in their 10 Å (a) and 7 Å (b) states.

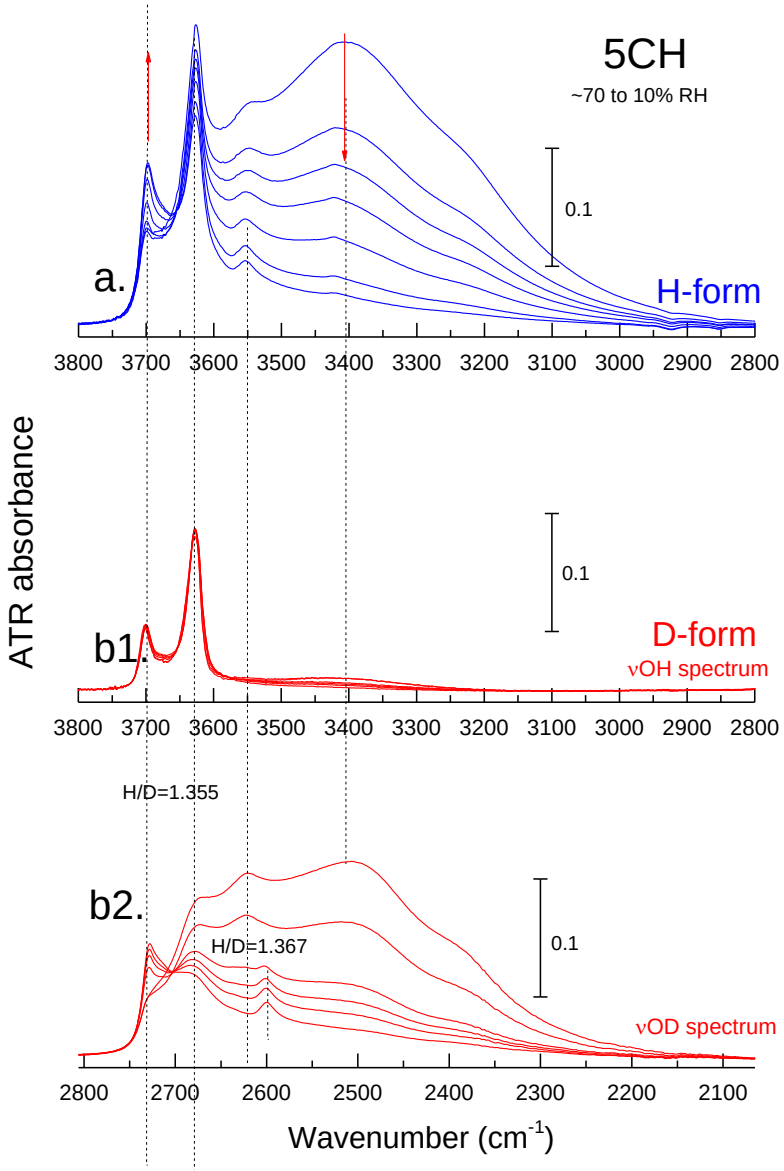

Figure S3. Detail of the ATR spectra monitoring the vO-H range during the -(10 Å) to –(7 Å) transition in cylindrical halloysite 5CH. For experimental details, see text. (b1, b2) The spectrum of the –(10 Å) end-member of each series is shown with a thick line. The vOD range of the D-form (b2) is shown with the x-axis expanded by a factor of 1.355 to facilitate comparison with the vOH spectra of both, the H- (a) and the D-forms (b1). Vertical bars indicate the y-axis scale of the spectra

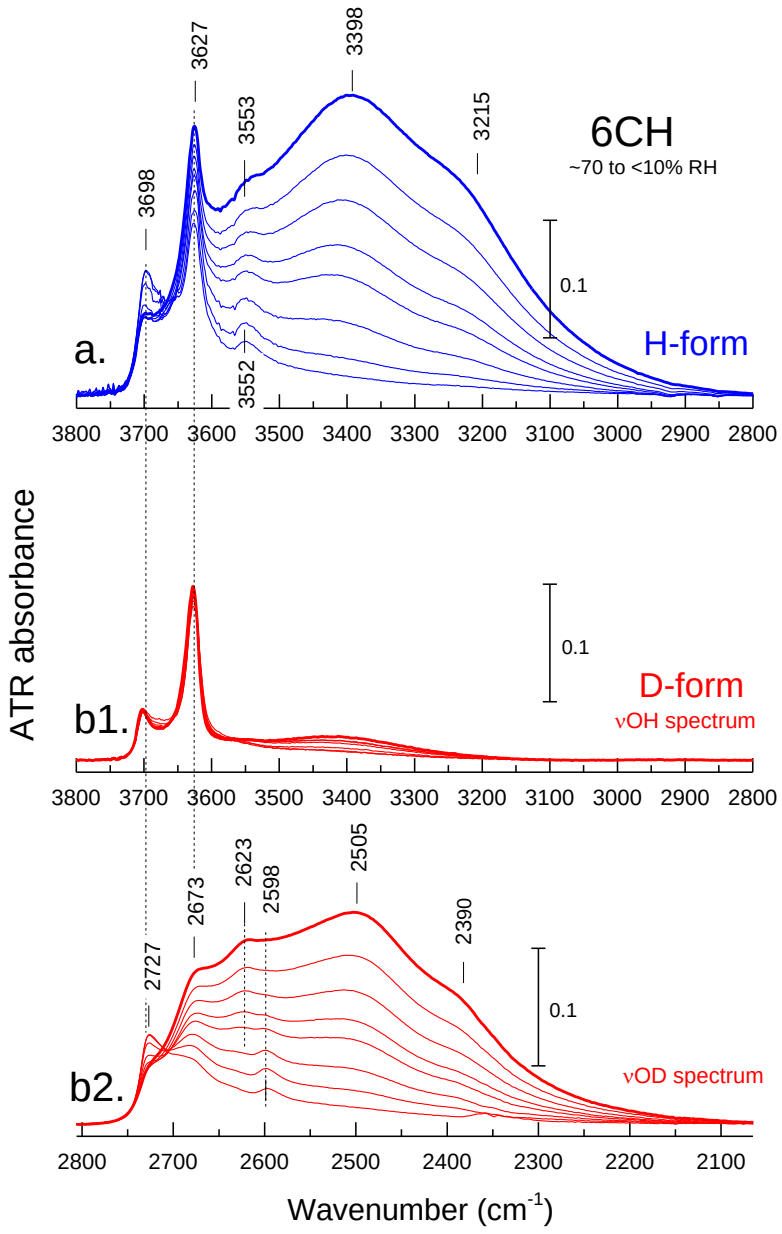

Figure S4. Same as Fig. S3 the -(10 Å) to –(7 Å) transition in cylindrical halloysite 6CH.

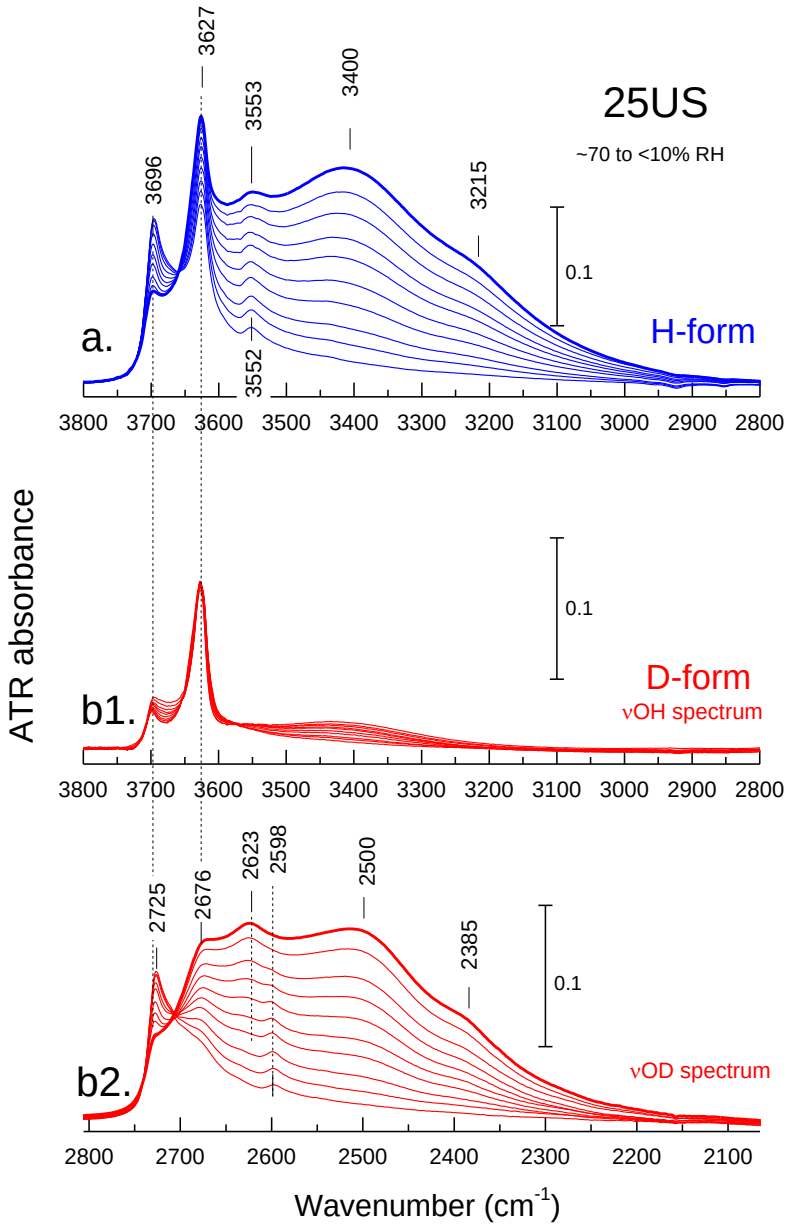

Figure S5. Same as Fig. S3 the -(10 Å) to –(7 Å) transition in cylindrical halloysite 25US.

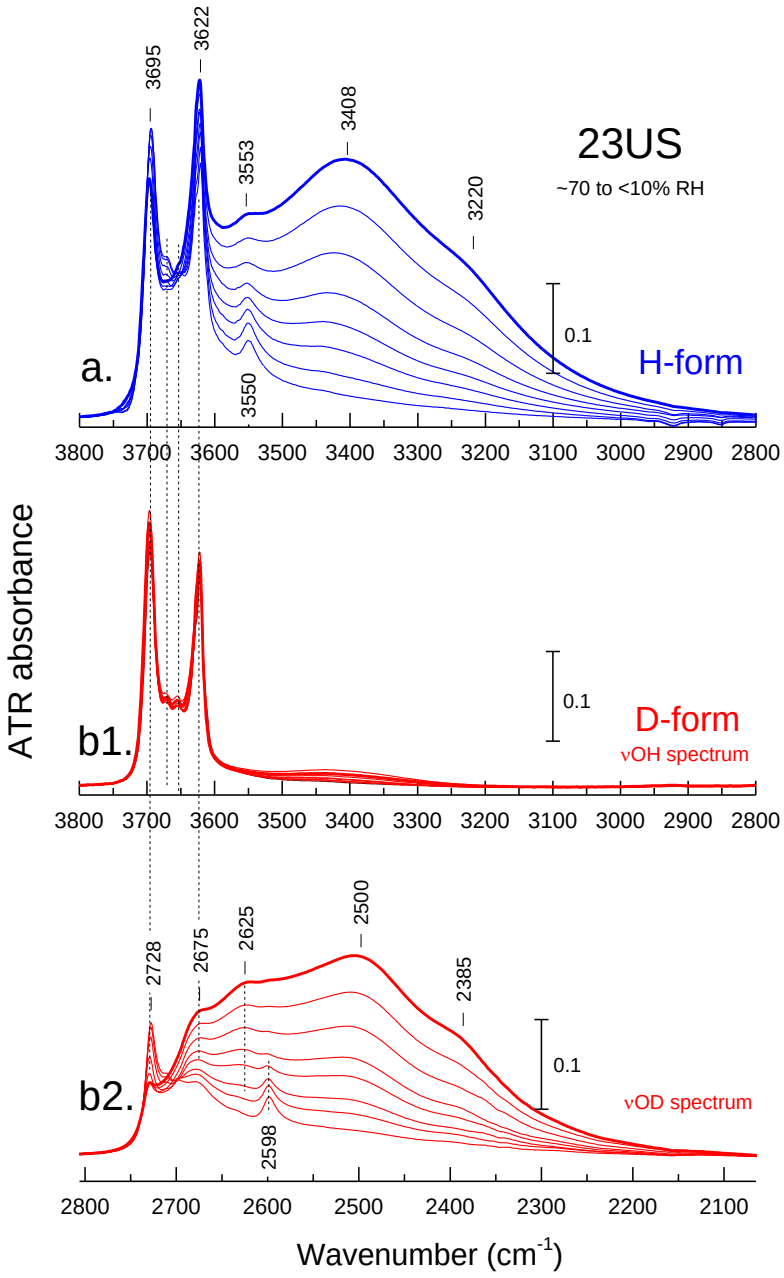

Figure S6. Same as Fig. S3 the -(10 Å) to –(7 Å) transition in polygonal halloysite 23US.

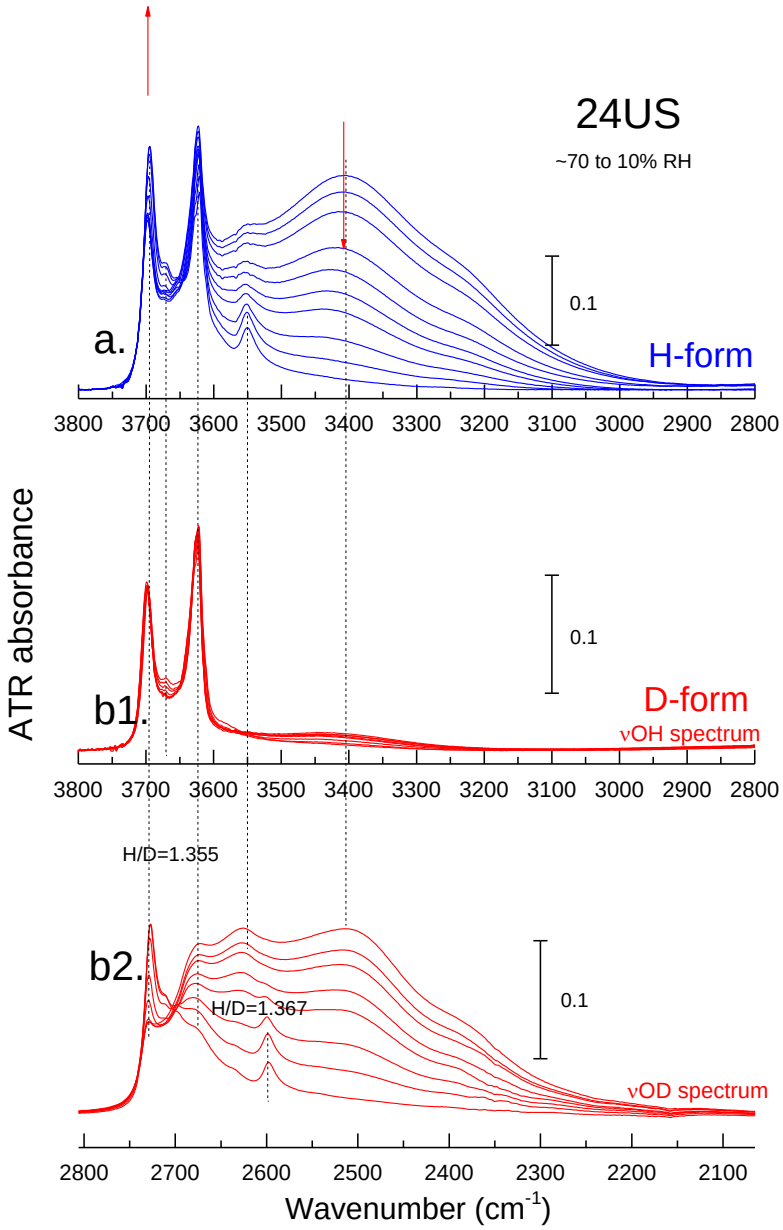

Figure S7. Same as Fig. S3 the -(10 Å) to –(7 Å) transition in polygonal halloysite 24US.

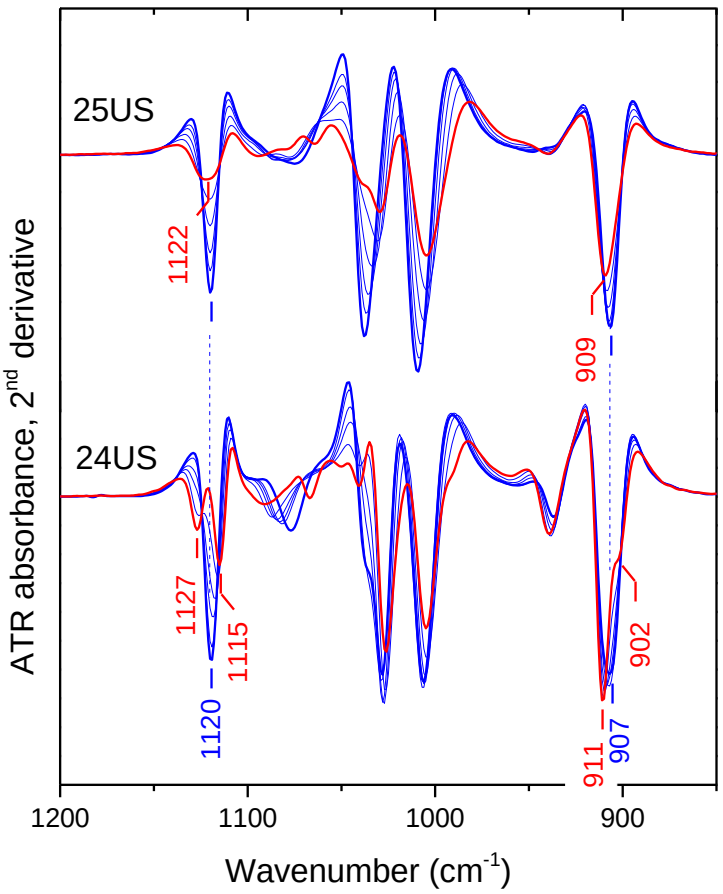

Figure S8. 2nd derivative (Savitzky-Golay, 9pt) evolution during the 10 to 7 Å conversion of polygonal 24US and cylindrical 25US halloysites. The spectrum of the 7 Å end member is shown in red. Peak positions are indicated for the ~1120 (Si-O) and the ~910 cm-1 (inner OH) modes. The data are taken from the H_2O series, but their D_2O counterparts are identical. Re-wetting of the 7 Å phase leaves the spectra of the 7 Å end-member unaffected.

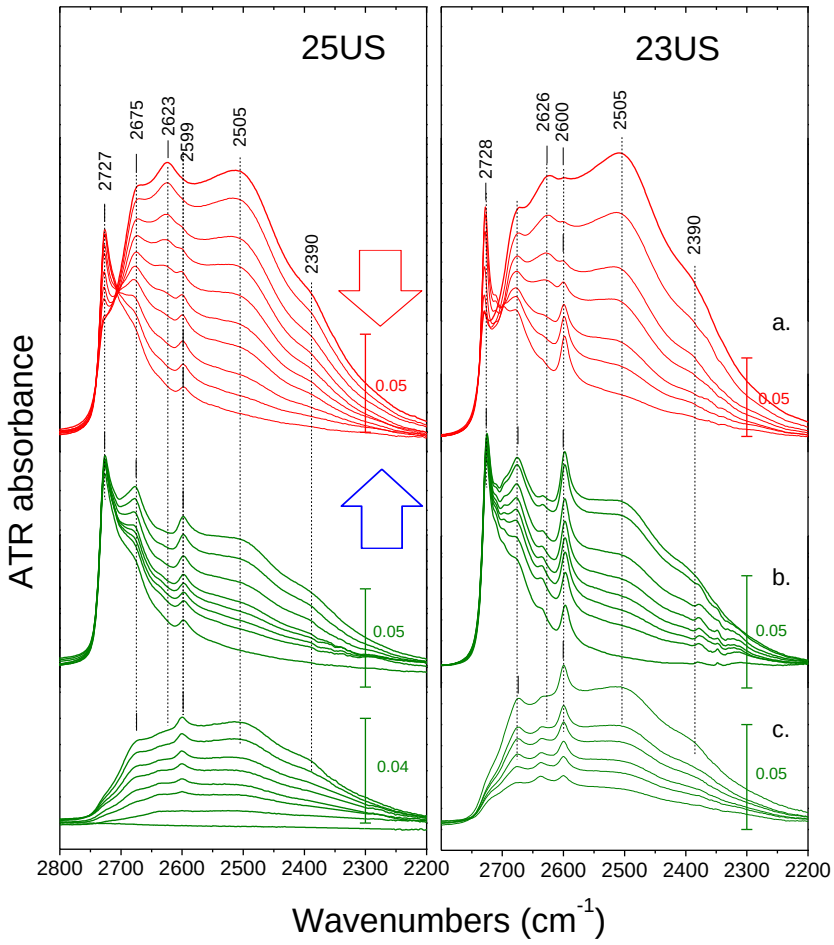

Figure S9. Detail of the ATR spectra monitoring the vO-D range in cylindrical halloysite 25US (left) and polygonal halloysite 23US (right) during: a. the transition D-halloysite-(10 Å) to –(7 Å); b. the rehydration of D-halloysite-(7 Å) by D_2O; c. the rehydration of H-halloysite-(7 Å) by D_2O. Vertical bars indicate the y-axis scale of the spectra in each panel.

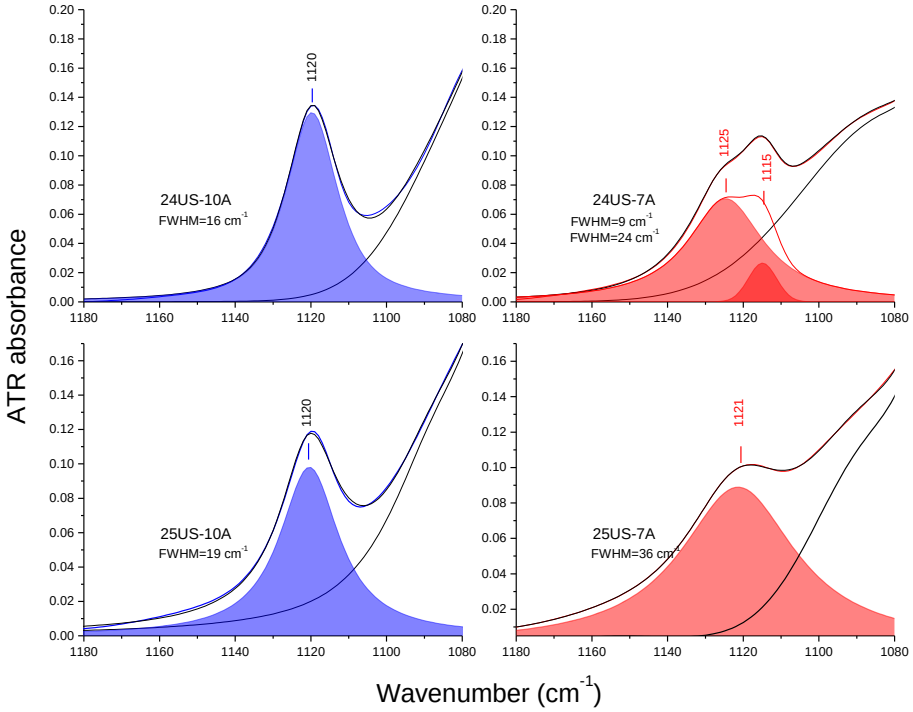

Fig. S10. Band fitting analysis of the ~1120 cm^{-1} mode in 24US (upper) and 25US (lower) in their 10 Å and 7 Å states (left, and right, respectively).

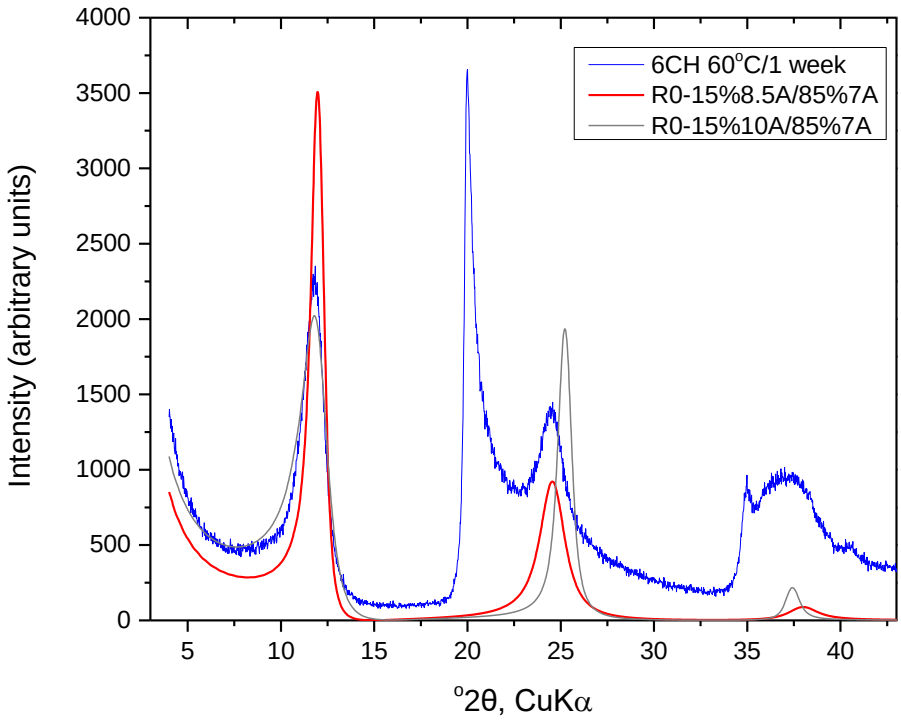

Fig. S11. Experimental (blue) and model patterns of 6CH-(7 Å) prepared by heating the 10Å starting material at 60 °C for 1 week. The consideration of 8.5 Å instead of 10 Å R0 interstratifications (red and grey, respectively) improves the simultaneous matching of the ~7.4 and 3.6 Å peak positions. Various other fits using an R0 interstratification of just 10 and 7 Å layers in different proportions were trialed, but none appears as satisfactory as those composed of 8.5 and 7 Å layers for the example shown. Undoubtedly, further improvement would result if a three-component system were used and it is also clear that elements of R1 segregation in a 3-component system will be required to match some of the profiles recorded at other stages of the dehydration, such as those shown in Figure 2. Modelled patterns were calculated manually using Sybilla v2.2.14.